https://doi.org/10.5194/egusphere-2025-4271
Preprint. Discussion started: 12 September 2025

The role of shear zones, faults and the associated fractures on the formation and character of bedrock surface depressions in crystalline bedrock (Turku, southwestern Finland)

Eemi Ruuska[1], Pietari Skyttä1, Kati M. Ahlqvist[2], Nicklas Nordbäck[2], Pelayo Barron[3], Kaisa Nikkilä[3]

[1] University of Turku, Department of Geology and Geology, Turku, Finland
[2] Geological Survey of Finland, Espoo, Finland
[3] Åbo Akademi University, Department of Natural and Health Sciences, Turku, Finland

Corresponding author: Eemi Ruuska (eeolru@utu.fi)

Abstract

Surface morphology of the crystalline bedrock is controlled by brittle bedrock structures, and while the contribution of the large-scale structures such as shear zones and faults are acknowledged, the contribution of detailed brittle structures associated to large-scale structures is more often overlooked.

In this study, multi-scale analysis of brittle structures and detailed 3D-modelling provide improved knowledge how the detailed brittle structures contribute on the formation and character of the bedrock surface depressions.

While the shear zones, faults and elongated bedrock depressions show parallel trends and overlap, the outcrop-scale fractures largely determine the dimensions and detailed surface morphology of the bedrock depressions. The surface morphology and orientation of bedrock depressions along shear zones and faults are contrasting particularly due to the strong ductile precursor associated with the shear zones and their lack for faults. However, for both the shear zones and faults, localized brittle deformation controls the generation of outcrop-scale fracture, which further controls the detailed surface morphological signatures along the elongated bedrock depressions, and particularly in their damage zones.

This study provides new insights into the detailed bedrock structures, that contribute to the development of complex bedrock surface morphologies within the bedrock surface depressions which are controlled by the brittle deformation and kinematics along the underlying shear zones and faults.

https://doi.org/10.5194/egusphere-2025-4271
Preprint. Discussion started: 12 September 2025

1. Introduction

Bedrock surface depressions are characteristically formed along structural discontinuities within the crystalline bedrock, including fracture systems and diverse shear zones and faults (DesRoches et al., 2014; Eyles, 2012; Glasser et al., 1998; Gleeson & Novakowski, 2009; Ruuska et al., 2023; Skyttä et al., 2015). Shear zones and faults are characterized by rocks of high overall strain and dense fracturing, where the earliest fracture orientation is in many cases inherited from older ductile structures (Crider, 2015; Mancktelow & Pennacchioni, 2005; Regenauer-Lieb & Yuen, 2008; Skyttä & Torvela, 2018). Subsequent glacial erosion, such as quarrying (plucking), abrasion and glacial ripping, utilizes the most preferential fracture orientation to generate elongate depressions along the eroded bedrock surface, which, consequently, contributes to their morphology (Bukhari et al., 2021; Dühnforth et al., 2010; Glasser et al., 2020; Krabbendam et al., 2022). As the bedrock surface functions as a depositional basement for younger sediments, the elongate depressions are overlain by unusually thick sedimentary overburden, and consequently, detailed knowledge about the bedrock surface morphology and the geological structures within the crystalline bedrock is not available (Ruuska et al., 2023). Some documented cases (Lane et al., 2015; Scott & Wohl, 2019; Skyttä et al., 2023) show that the orientation of fault (or shear zone) surfaces and related fractures observed at the outcrop-scale are the main controlling geological feature over the morphology of the fault-related elongate bedrock depressions. As several studies have shown that the characteristics of the bedrock are scalable from individual outcrops to regional extent (Bertrand et al., 2015; Hall & Gillespie, 2017; Kirkpatrick et al., 2013; Nordbäck et al., 2023; Samsu et al., 2020) it is justified to complement the gaps between the scales and correlate individual fractures to larger brittle features in the bedrock, including the gaps associated with the covered bedrock surface depressions. Scalability is particularly valid for analysing length and orientation distributions of the fracture networks (Chabani et al., 2021; Dichiarante et al., 2020; Hardebol et al., 2015), and also for topological properties of the contained fractures (Ovaskainen et al., 2022; Sanderson & Nixon, 2015).

The landscape of Turku (SW Finland) is characterized by abrupt changes in topography, which reflects heterogeneous glacial erosion that was imposed upon the highly variable bedrock in terms of both the lithology and the bedrock surface morphology (Hietanen, 1947; Niemelä et al., 1987; Ahlqvist et al., in prep.). The roughness of the bedrock surface topography is attributed to the presence of an elongate ENE-striking bedrock depression system generated by either one set or repeatedly cross-cutting sets of shear zones (Härme, 1960; Niemelä et al., 1987; Väisänen & Hölttä, 1999). This pattern is supported by the elongate depressions recently recognized from new and comprehensive digital elevation model of the eroded bedrock surface (bedrock-DEM) compiled for the Turku region by Ahlqvist et al., in prep. However, no studies illustrate how the bedrock structures, ranging from ductile to brittle deformation and, including the variation in spatial occurrence and intensity, contribute to the development of the heterogeneous bedrock surface topography. The most prominent elongate depressions are asymmetric (Ahlqvist et al., in prep.), but the causes of the asymmetry in the underlying bedrock remain uncharacterized.

https://doi.org/10.5194/egusphere-2025-4271
Preprint. Discussion started: 12 September 2025

In this paper we show how the occurrence and morphology of the bedrock depressions are controlled by brittle deformation localized in shear zones (foliation-parallel) and faults (foliation-discordant). We show that the ductile structures do not appear to control the generation of the brittle structures as dominantly as suggested in the literature. To justify the above statements, we provide structural data over the relationship of the structures in two different scales and highlight the role of the brittle faults and the associated fracture patterns, in controlling the morphology of the bedrock surface topography. Our approach focuses on variations in geometry and strain associated with the ductile deformation (high- and low-strain domains), and the systematics of brittle fractures including orientation, intensity and topology analysis, and correlation with the ductile domains. This characterization of the bedrock structures supports our 3D-interpretation of the structurally constrained bedrock surface with detailed analysis along cross-sections and a photogrammetry model. These detailed analyses provide significant knowledge for recognizing i) the morphological variations of the bedrock surface within the shear zones and faults, ii) the most effective fracture orientations contributing to the bedrock surface morphology within the damage zone of shear zones and faults, and iii) the significance of the analyses of the bedrock structures for generating geologically realistic 3D-interpretations within sediment-covered areas.

2. Geological setting

The bedrock of the study area is within the southwestern part of the Southern Finland Subprovince (SFS) formed and modified during the 1.9–1.8 Ga Svecofennian orogeny (Bogdanova et al., 2015; Hermansson et al., 2008; Lahtinen et al., 2009;Nironen, 2017). The lithology of the study area is characterized by late orogenic s-type granites and associated migmatites (1.84-1.83 Ga; Huhma, 1986; Suominen, 1991; Ehlers et al., 1993; Korsman et al., 1997; Väisänen & Hölttä, 1999; Kähkönen, 2005; Kurhila et al., 2005).

Four major deformation phases (D1-D4), and associated structures have been recognized in the western part of the SFS (Väisänen & Hölttä, 1999). D1-structures comprise a biotite foliation parallel with the primary bedding, deformed during the later deformation phases (Väisänen & Hölttä, 1999). These structures were deformed by the D2 to tight to isoclinal folds with sub-horizontal axial planes (Väisänen & Hölttä, 1999). D3 included intensive NW-SE shortening, causing refolding the early D1/D2 structures into E- and NE-trending upright to overturned isoclinal structures (Väisänen & Hölttä, 1999) and contributed to further thickening of the crust at 1.84-1.83 Ga (Ehlers et al., 1993). Together with the sub-horizontal or moderately plunging fold axes, steep fold axes exist on the limbs of the regional folds, together forming dome-basin structures (Väisänen & Hölttä, 1999). The intensity of D3-folding varies as shown by the variation from isoclinal to open folds with occasional sheared fold limbs. D4-structures are N- to NE-trending localized shear zones, which show both brittle and ductile deformation features, and cross-cut and deflect older structures (Väisänen & Hölttä, 1999; Väisänen & Skyttä, 2007).

https://doi.org/10.5194/egusphere-2025-4271
Preprint. Discussion started: 12 September 2025

The earliest shear zones were generated during the D3-stage on the limbs of the folds, and they show parallel orientation with the general D3 structural trends (Hietanen, 1947; Väisänen & Hölttä, 1999). The major shear zones in the southwestern Finland form a pattern where the shorter ~NE-trending Mynälahti Shear Zone (MSZ) and Paimio Shear Zone (PSZ) abut to the 150-200 km long ~E-trending Somero Shear Zone (SSZ) in the north and to the Southern Finland Shear Zone (SFSZ) in the south (Fig 1; Nordbäck et al., 2023; Torvela & Ehlers, 2010; Väisänen & Skyttä, 2007). The SFSZ and SSZ are dextral strike-slip faults, whereas the NE-trending ones are dip-slip in character (Väisänen & Skyttä, 2007). The main deformation within these contractional shear zones took place at 1.83–1.82 Ga (Torvela et al., 2008; Väisänen & Skyttä, 2007). The earlier ductile reverse slip along the abutting NE-trending zones during the transpression was followed by, E-side down, normal slip, which demonstrates a fundamental change in the orogeny from the compressional to the extensional setting at around 1.79 Ga (Väisänen & Skyttä, 2007). The sub-vertical NE-trending Airisto Shear Zone (ASZ), characterized by dip slip kinematics (Simelius, 2013), is likely also related to extensional phase. According to Torvela & Kurhila, (2022), the extensional phase may have been transient at 1.82-1.81 Ga, and followed by dominant strike-slip shearing at 1.80-1.79 Ga. The age of shearing remains to be discussed, but the MSZ close to the Vehmaa rapakivi granite is overprinted by post-tectonic micas indicates that the faulting preceded the rapakivi magmatism and controlled the emplacement of the post-orogenic granitoids (Väisänen & Skyttä, 2007).

Multistage evolution of the brittle structures has been acknowledged in the southwestern part of SFS (Mattila & Viola, 2014; Nordbäck et al., 2024)including; i) onset of the brittle deformation in the NW-SE compression c. 1.75 Ga, ii) the N-S oriented transpressional compression shortly after, iii) NW-SE extension during the rapakivi magmatism around 1.64 Ga, iv) WNW-ESE to NNW-SSE compression, which reactivated the NE-SW trending shear zones and generated E-W trending strike-slip faults around 1.55-1.4 Ga, v) NE-SW compressional stage around 1.3-1.2 Ga, and vi) NW-SE to ENE-WSW compression during the Sveconorwegian orogeny.

In their recent bedrock-DEM modelling, Ahlqvist et al., (2025) recognized the presence of several bedrock surface depressions, which they further categorized into six groups based on their trend (I-VI; Fig. 1c). Depressions of the Group I strike ENE across the study area in the central part along the Aura River, where they generate most significant contrast in the bedrock elevation. The eastern part of the study area is featured by several shorter, NW-trending, bedrock depressions (Group II), whereas the Group III is featured by a distinct NE-trending depression separating the mainland and archipelago within the study area. The southern and northern parts of the study area include individual bedrock depressions belonging into Group IV, V and VI (Fig. 1c), which show only minor contribution to the bedrock surface topography. Thus, bedrock topography is primarily controlled by the intersecting and abutting bedrock depressions of Groups I, II and III which are concordant with the regional foliation.

https://doi.org/10.5194/egusphere-2025-4271
Preprint. Discussion started: 12 September 2025

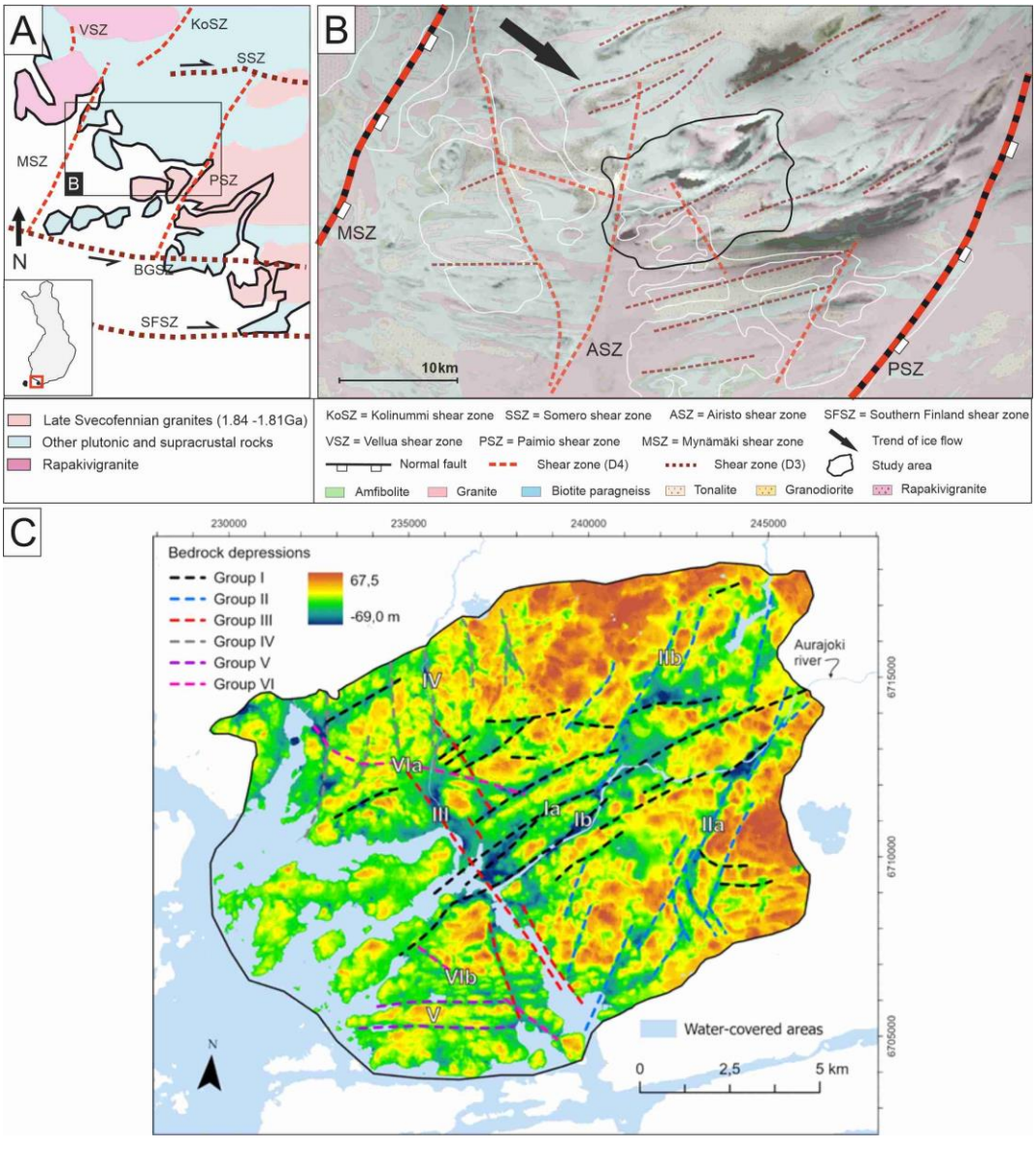

Figure 1: A) The main shear zones and the generalized bedrock lithology of southwestern Finland. B) More detailed structural and lithological setting around the study area. Bedrock of Finland map (1:200k; Geological survey of Finland (GTK)) and low-altitude aeromagnetic map (GTK) in the background C) The bedrock surface elevation model and main bedrock depressions by Ahlqvist et al., 2025.

130

https://doi.org/10.5194/egusphere-2025-4271
Preprint. Discussion started: 12 September 2025

3. Data and methods

The used approach comprises: i) Method-specific structural analysis in a regional-scale from remote sensing data together with the outcrop-scale analysis from 2D-photogrammetry and field mapping measurements. ii) Bedrock surface modelling including re-generation and improvement of bedrock-DEM from regional to detailed scale. iii) Development of a structural synthesis, which binds together the results of method-specific structural analyses and bedrock surface modelling by emphasizing the correlation between structural features observed from remote sensing, field mapping and bedrock surface models.

3.1 Method-specific structural analysis

The structural analysis aimed at defining the geometrical framework of both the ductile and brittle structures within the study area. The remote sensing data was used to compile 2D form line interpretations of foliation, folds, shear zones and faults, and Lidar-based lineament interpretation of linear brittle features of the bedrock. In the analysis, we used aeromagnetic maps for 2D form lines (Geological survey of Finland) and ground surface elevation LiDAR (National Land Survey of Finland) for lidar lineaments supported by field observations.

During the field mapping, we investigated 152 horizontal and vertical bedrock exposures and collected foliation and fracture (including outcrop walls) measurements. The foliation was classified into low- and high-strain (gentle and sub-vertical dip angle, respectively) domains along the cross-section-DEM. Fractures, observed both as traces and exposed fracture-controlled outcrop walls, were divided into major (R1), and minor (R2) groups based on their intensity on each individual outcrop. The number of sub-horizontal fractures is limited due to the scattered locations of the vertical outcrops. We used both the field measurements and the remote sensing data (LiDAR, aeromagnetic maps) in an integrated way to generate two separate thematic interpretations, which emphasize the characteristic ductile trends (form lines) and brittle discontinuities (Lidar lineaments) of the bedrock.

The 2D-photogrammetry model was generated for analysing the fracture orientation and topology, and compare the results to the overall fracture pattern and orientation of the bedrock depression within the study area, with a particular focus on the bedrock depression along the Aura River (Fig. 1c, 2). The 2D-photogrammetry model contains merged photographs taken by drone from 20m high covering the area of c. 100x100m. 1185 fracture traces were manually digitized on the 2D-photogrammetry model and nodes of the fracture topology are interpreted by using NetworkGT-plugin (Nyberg et al., 2018) in the QGIS software.

https://doi.org/10.5194/egusphere-2025-4271
Preprint. Discussion started: 12 September 2025

3.2 Bedrock surface modelling

Data of the bedrock surface elevation is based on geotechnical drillings in the covered areas and bedrock outcrop elevation points from ground surface LiDAR (Ahlqvist et al., 2025). For honouring the effect of the continuous 2D form lines to bedrock surface within the sea area, we added dummy points (Fig. 2a) to lower the elevation of the high bedrock surface interpretation at areas which lack geotechnical drilling data. Elevation of the control points are set to -40 m.a.s.l at sea and -15 m.a.s.l in a small area of land along ASZ. We also added seven control points between -15 and -16 m.a.s.l for covering the data gaps in the SE part of the study area (Fig. 2). Depth of the dummy points is set based on estimated thickness of the sediment deposits in the bedrock depressions within the study area.

We generated three bedrock surface models (Fig. 2) including i) the bedrock-DEM showing the bedrock surface elevation within the whole study area, and two cross-section-DEMs across ii) the central part of the study area (T1-DEM), and iii) the SE part of the study area (T2-DEM). The bedrock-DEM and the cross-section-DEMs are generated in MOVE Suite (3D-modelling software provided by PE Limited) using the Ordinary Kriging (OK) interpolation method The OK interpolation is guided by the semivariogram (Fig. 2), which measures the average degree of dissimilarity between unsampled values and nearby values (Davis, 2002; Krivorucko & Gotway, 2004).

The bedrock-DEM was interpolated using a 30m-grid and exponential experimental model giving a highly accurate fit for the variogram model of our data (Fig. 2x). The honour points -method in MOVE increases the accuracy into 10m-grid in areas, where the elevation of the bedrock surface exposure is obtained from ground surface LiDAR data (Fig. 2x).

The cross-section-DEMs were interpolated (T1-DEM & T2-DEM) using 10m-grid size with increased accuracy of 2-5m on the areas, where the bedrock elevation is detected from ground surface LiDAR data. The data of the bedrock surface elevation and bedrock structures was selected within 750m distance from Trace 1 for the T1-DEM, while the data for T2-DEM covers the area of c. 3000x5000m in the SE part of the study area (Fig. 2). Best-fit interpolation was reached using exponential experimental model in both cross-section-DEMs, in which detailed semivariogram settings were set separately due to different datasets (Fig. 2d,e). Cross-section of the T1-DEM concentrates in the variation in strain illustrated by the steepness of the foliation, and its interaction between the geometry of the shear zones and fracturing. Cross-section of the T2-DEM emphasizes the association between data coverage and analysis of the brittle structures for generating geologically realistic bedrock surface morphology.

3.3 Structural synthesis

As the final step of the analysis, we compiled structural synthesis to show how the bedrock structures affect to the bedrock surface morphology. General setting of bedrock structures was determined as the compilation of shear zones and faults as 2D form lines, brittle structures as Lidar-lineaments and fracture field data. The bedrock depressions were interpreted from the bedrock-DEM and compiled with the general setting of the bedrock structures to provide more accurate precision to locate

https://doi.org/10.5194/egusphere-2025-4271
Preprint. Discussion started: 12 September 2025

major structural features of the bedrock such as shear zones, faults and continuous LiDAR-lineaments. This approach was taken into more detailed scale within the cross-section-DEMs, where the relationship between detailed bedrock surface morphology, and Lidar-lineaments and fractures was analysed near the major structural features. Lastly, based on the compilation of bedrock structures and detailed analyses within the cross-section-DEMs, we generated final structural synthesis that provided complex network of shear zones, faults and associated brittle structures which affect to bedrock surface morphology.

https://doi.org/10.5194/egusphere-2025-4271
Preprint. Discussion started: 12 September 2025

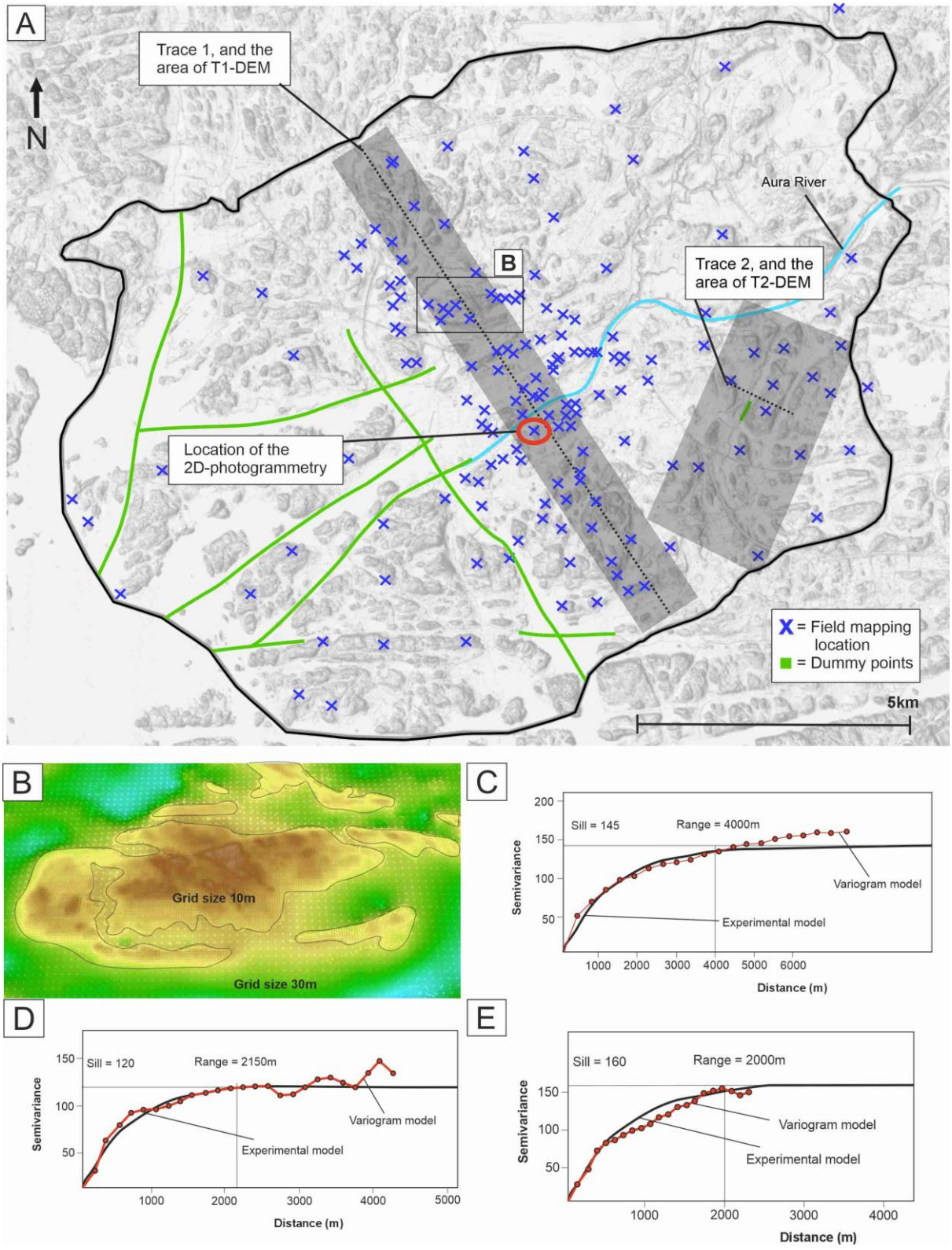

Figure 2. A) Borders of the study area and location of the field mapping outcrops, dummy points, cross-section-DEM areas and Traces, and 2D-photogrammetry model. Ground surface elevation LiDAR on the background (National Land Survey of Finland). B) Interpolation of bedrock surfaces with differing grid sizes (Honour points -method in OK interpolation in MOVE). C) Semivariogram of the bedrock-DEM. D) Semivariogram of the T1-DEM. E) Semivariogram of the T2-DEM.

https://doi.org/10.5194/egusphere-2025-4271
Preprint. Discussion started: 12 September 2025

4. Results

4.1 Distributed ductile structures

The ductile structure is dominated by subvertical ENE-striking foliation, which shifts more towards E-striking in the south (Fig. 3). The foliation is intense near the deformation zones and fold structures, and weak especially within the domain covered by metavolcanic rocks further away from deformation zones. Based on the fold geometries and the resulting dip variation of the folded foliation, the study area could be subdivided into low- and high-strain domains with respect to the distributed ductile deformation. The low-strain domain is defined by an open upright antiform with sub-horizontal west-plunging fold axis within the central part of the study area (Fig. 3,4). High-strain domains occur throughout the study area as illustrated by subvertical foliation particularly near the deformation zones (Fig. 4a). High-strain domains include tight to isoclinal folds with subvertical limbs and narrow hinge zones most representatively displayed by the synform-structure on the southern side of the low-strain domain.

4.2 Localized deformation: Shear zones and faults

Three shear zones and two faults were distinguished within the study area (Fig. 3). Shear zones SZ1-3 have subparallel trends with each another and the regional foliation, whereas faults F1 and F2 intersect the foliation (Fig. 3). The ENE-striking SZ1 and SZ2 are the most distinct shear zones with a continuation across the whole study area. These shear zones are subparallel with the lithological boundaries of the bedrock, which is dominated by metavolcanic rocks in the south and biotite paragneisses in the north. The discontinuous SZ3 strikes E-W, thus corresponding to the shift of the foliation trend from ENE to E-W towards south. F1 strikes NW and extends beyond the study area in the north. In the central part of the study area, F1 cross-cuts SZ1, SZ2 and the synform, and abuts to the open antiform-structure within the low-strain domain (Fig. 3). F2 is a shorter NE-striking feature that extends close to the SZ3 in the south, and abuts to the SZ1 in the north.

https://doi.org/10.5194/egusphere-2025-4271
Preprint. Discussion started: 12 September 2025

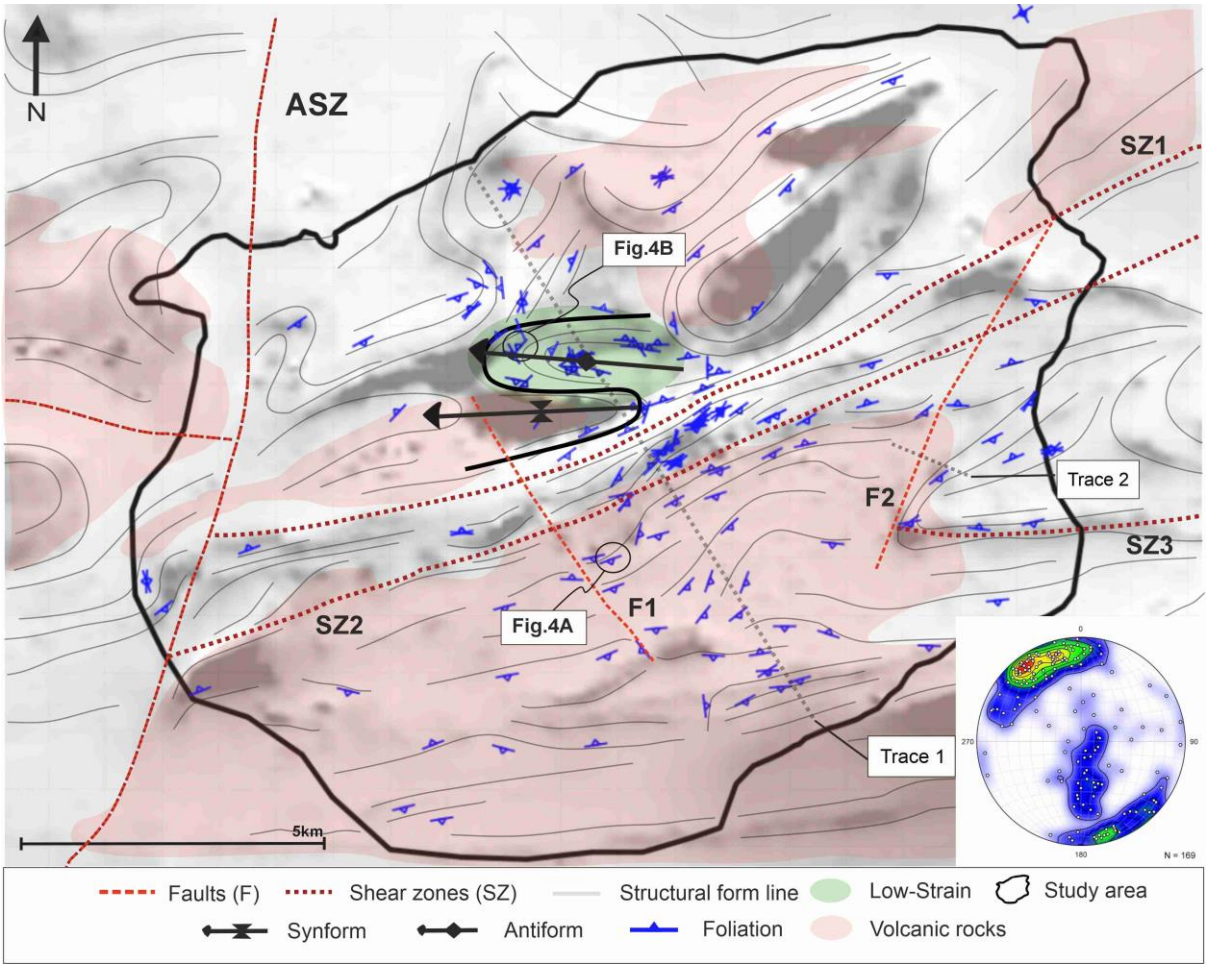

Figure 3. Shear zones, faults, foliation, fold structures (black line) and simplified lithology of the study area. Low-altitude aeromagnetic map on the background (Geological survey of Finland).

4.3 Outcrop fracture data

Fracture pattern on a typical outcrop comprises one major subvertical fracture orientation (R1), occurring either as an individual fracture or set of parallel fractures, often accompanied by at least one minor (R2) fracture set (Fig. 5). The R1-fractures feature either straight (Fig. 5a) or slightly undulating (Fig. 5b) in character, and often control the orientation of outcrop walls (Fig. 5c). While R1-fractures are continuous and regularly occurring on the outcrops, R2-fractures are short and they often abut to the R1-fractures (Fig. 5b,c). The NNE- to NNW-striking subvertical fractures are the most distinct R1 orientation, while the ENE-, NW- and E-striking subvertical fractures are more often categorized as R2-fractures (Fig. 6b-d).

https://doi.org/10.5194/egusphere-2025-4271
Preprint. Discussion started: 12 September 2025

The 2D-photogrammetry model shows similar fracture setting as the typical outcrops, where the major (R1) and minor fractures (R2) and their relationships are easily distinguished (Fig. 7a,b; R1=NNE-striking and R2=NW-striking). The NNE-striking fractures are +100m in length, and have an overall high intensity due to close spacing with approximately two fractures per metre. The minor fractures contain NW-striking fractures occurring throughout the area, whereas the N-striking fractures are limited to the northeastern and eastern parts of the outcrop in their occurrence. The NNE- and NW-striking fractures generate a fracture pattern, where the NW-striking fractures often abut to the NNE-striking ones (Fig. 7b). Within the well-exposed central parts of the 2D-photogrammetric model, high amount of Y- and X-nodes indicates that the fracture network is very connective. Furthermore, I-nodes are regular at borders of the outcrop and in such places, where the bedrock surface dips underneath the vegetation, which indicates that many of the I-nodes may well continue outside of the outcrop and underneath the vegetation.

https://doi.org/10.5194/egusphere-2025-4271
Preprint. Discussion started: 12 September 2025

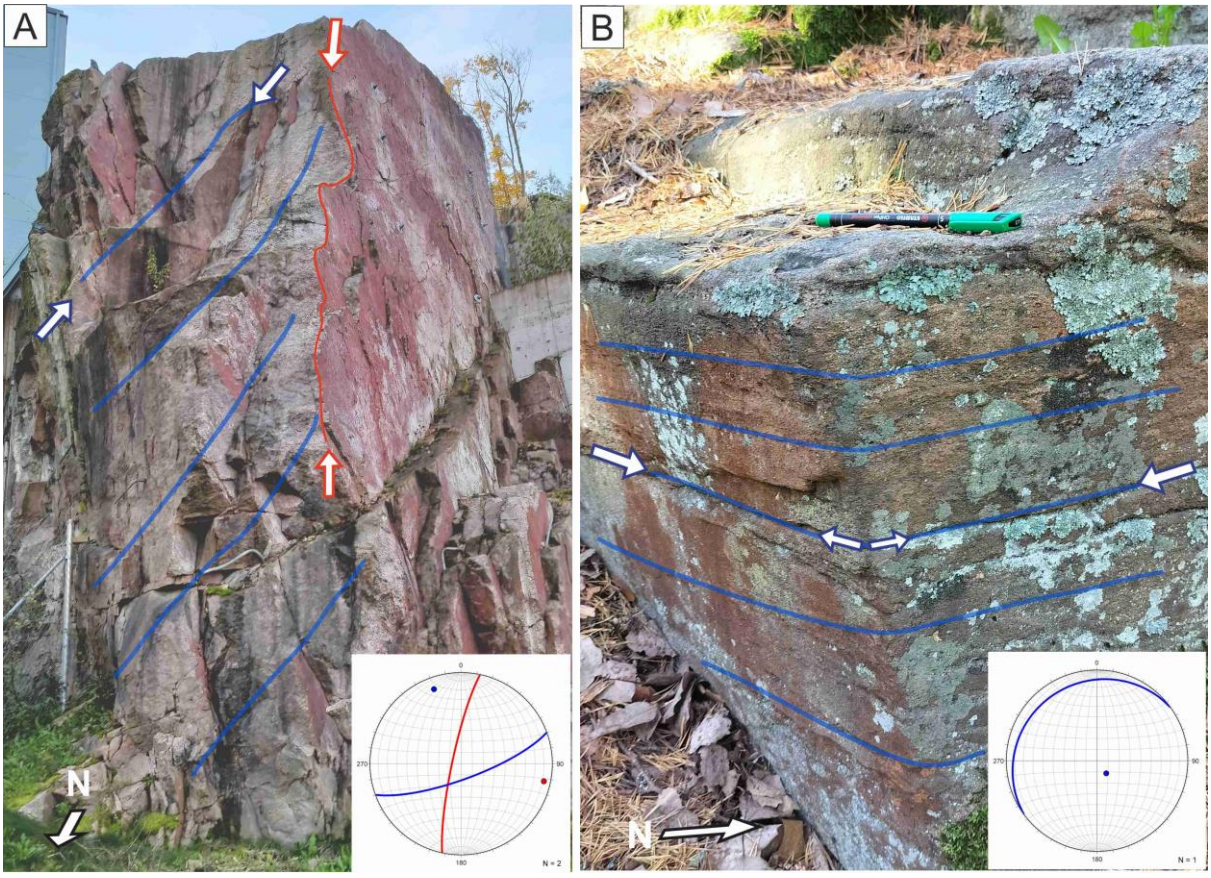

Figure 4. Typical subvertical foliation in high-strain areas (A), and subhorizontal foliation in low-strain areas (B). Blue lines imitate the foliation pattern in the outcrops. Red line emphasizes the major fracture orientation, which is obliquely oriented with the foliation orientation. Outcrop heights: 10m (A) and 1m (B). The outcrop in Fig. 4B is presented in a wider scale in the Fig. 5C.

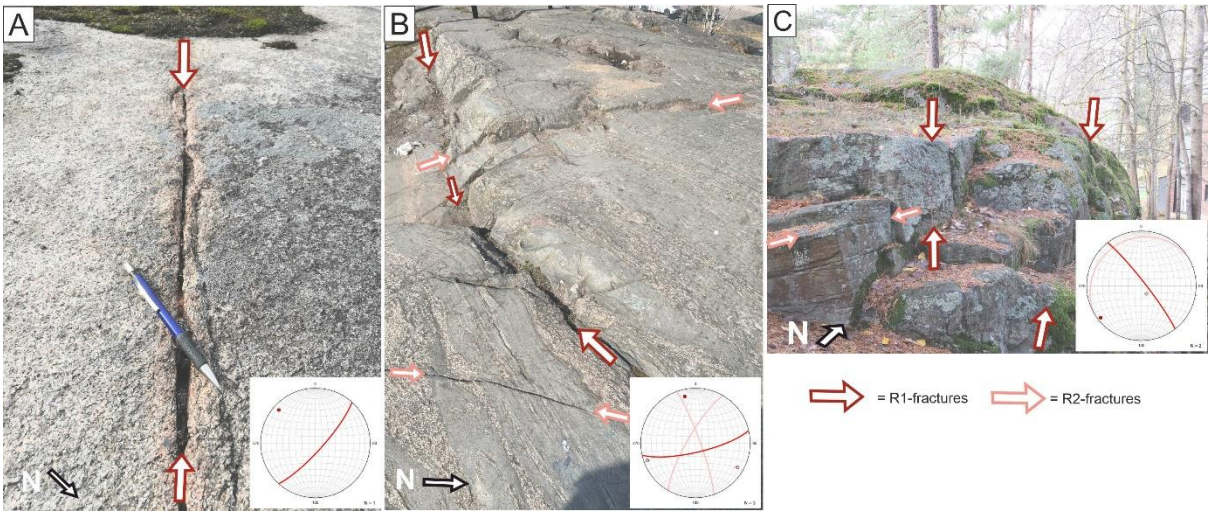

Figure 5. A) R1-fracture without R2-fractures. B) R1-fracture with two R2-fracture sets. C) Subvertical R1-fracture set generate distinct outcrops walls, while R2-fracture set is parallel with the sub-horizontal foliation.

https://doi.org/10.5194/egusphere-2025-4271
Preprint. Discussion started: 12 September 2025

4.4 Lidar lineaments

The most distinctive lineament sets interpreted throughout the study area strike ENE, NW and NNE to NE. The central part of the study area is characterised by the ENE-striking lineaments which show much sporadic appearance elsewhere as well as the E-striking lineaments show strong character only in the southern part. The lineaments striking NW are evident in the northwestern part of the study area, which accommodates highly variable and densely interpreted lineament system compared to other parts of the study area. The NNE- to NE-striking lineament trend is prevailing in the southeastern part of the study area. NW- and NNE- to NE-striking lineaments are more spatial distributed throughout the study area than the ENE- and E-striking lineaments.

4.5 Structural patterns of the bedrock-DEM

The elevation of the bedrock surface varies between 60 m below and 70 m above the sea level (-60 - 70 m.a.s.l) showing abrupt changes due to variously striking elongated bedrock depressions occurring throughout the bedrock-DEM (Fig. 8). Bedrock depressions show four orientation sets with ENE, NNE to NE, NW and E strikes. The ENE-striking bedrock depressions prevail the morphological features of the bedrock surface since they are crossing through the central and northern part of the study area creating sharp contrast to the bedrock elevation. The most common orientation of the bedrock depressions strikes NNE to NE (Fig. 9), but these depressions are narrow and discontinuous in morphological character compared to the ENE-depressions. The NW-striking bedrock depressions are mainly scattered in the north and south, but long NW-striking bedrock depression extends through the study area separating the mainland from archipelago, and turns more N-striking in the north. E-striking bedrock depressions are almost exclusively featured in the southern part of the study area.

https://doi.org/10.5194/egusphere-2025-4271
Preprint. Discussion started: 12 September 2025

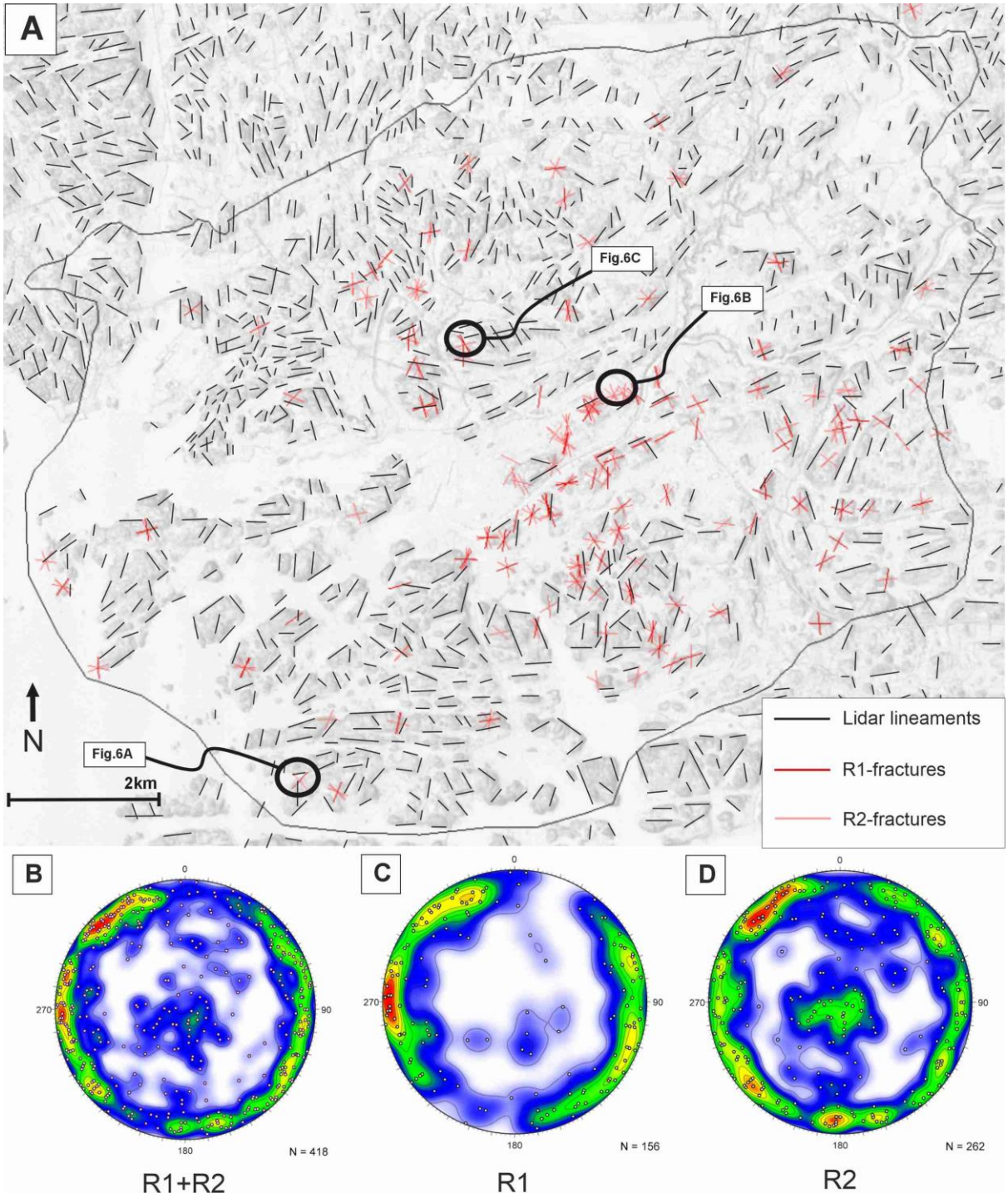

Figure 6. Brittle structures within the study area. A) Lidar lineaments and outcrop fractures. Ground surface elevation LiDAR on the background. Stereoplots represent all of the fractures (B), R1-fractures (C) and R2-fractures (D).

https://doi.org/10.5194/egusphere-2025-4271
Preprint. Discussion started: 12 September 2025

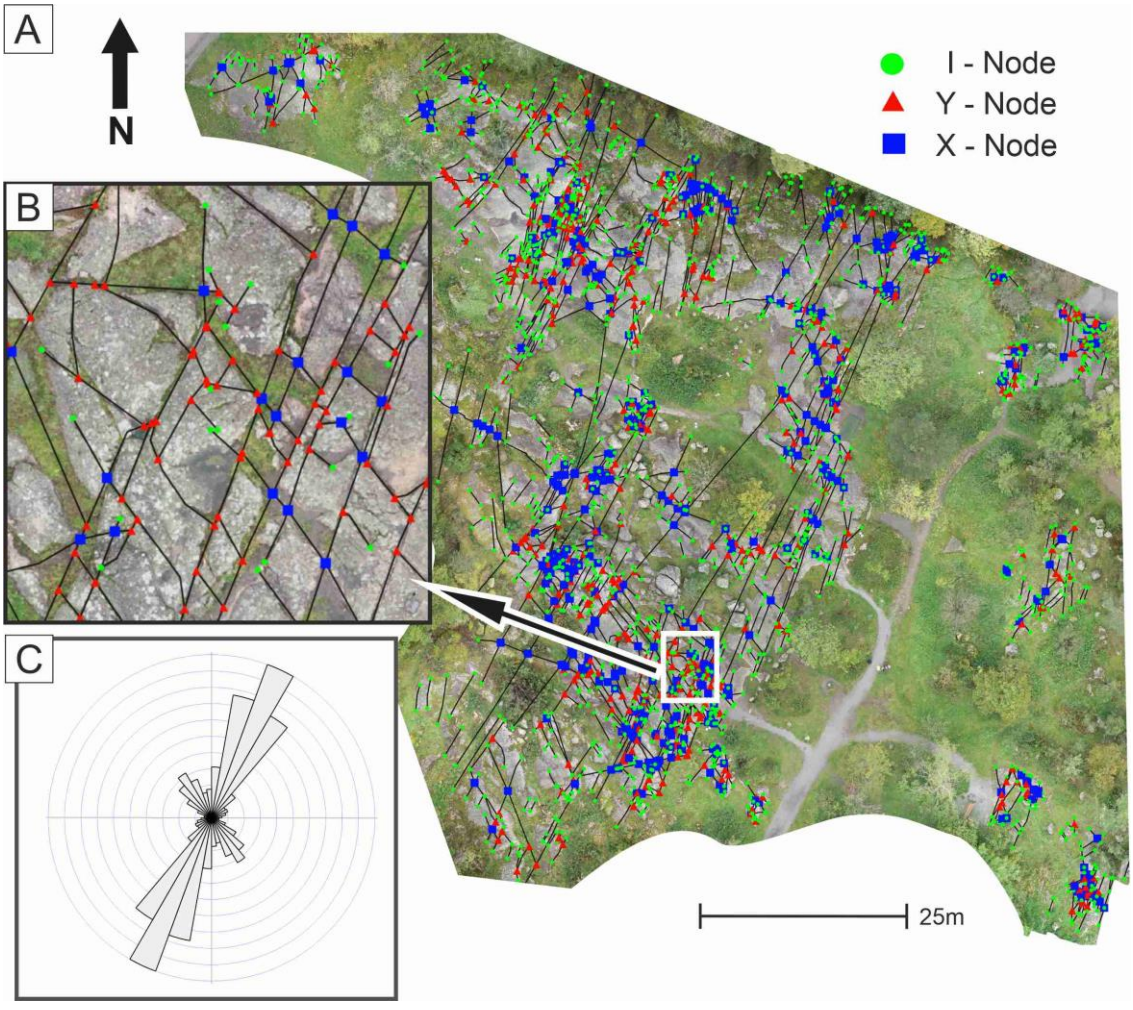

Figure 7. 2D-photogrammetry model. A) Outcrop of the 2D-photogrammetry with topological features (I, Y and X-nodes). B) Detailed image from the southern part of the outcrop illustrates the typical topological setting, in which NE-striking fractures often abut (Y-nodes) to the continuous NNE-striking fractures. C) Rose plot presenting a strike distribution of the fractures.

https://doi.org/10.5194/egusphere-2025-4271
Preprint. Discussion started: 12 September 2025

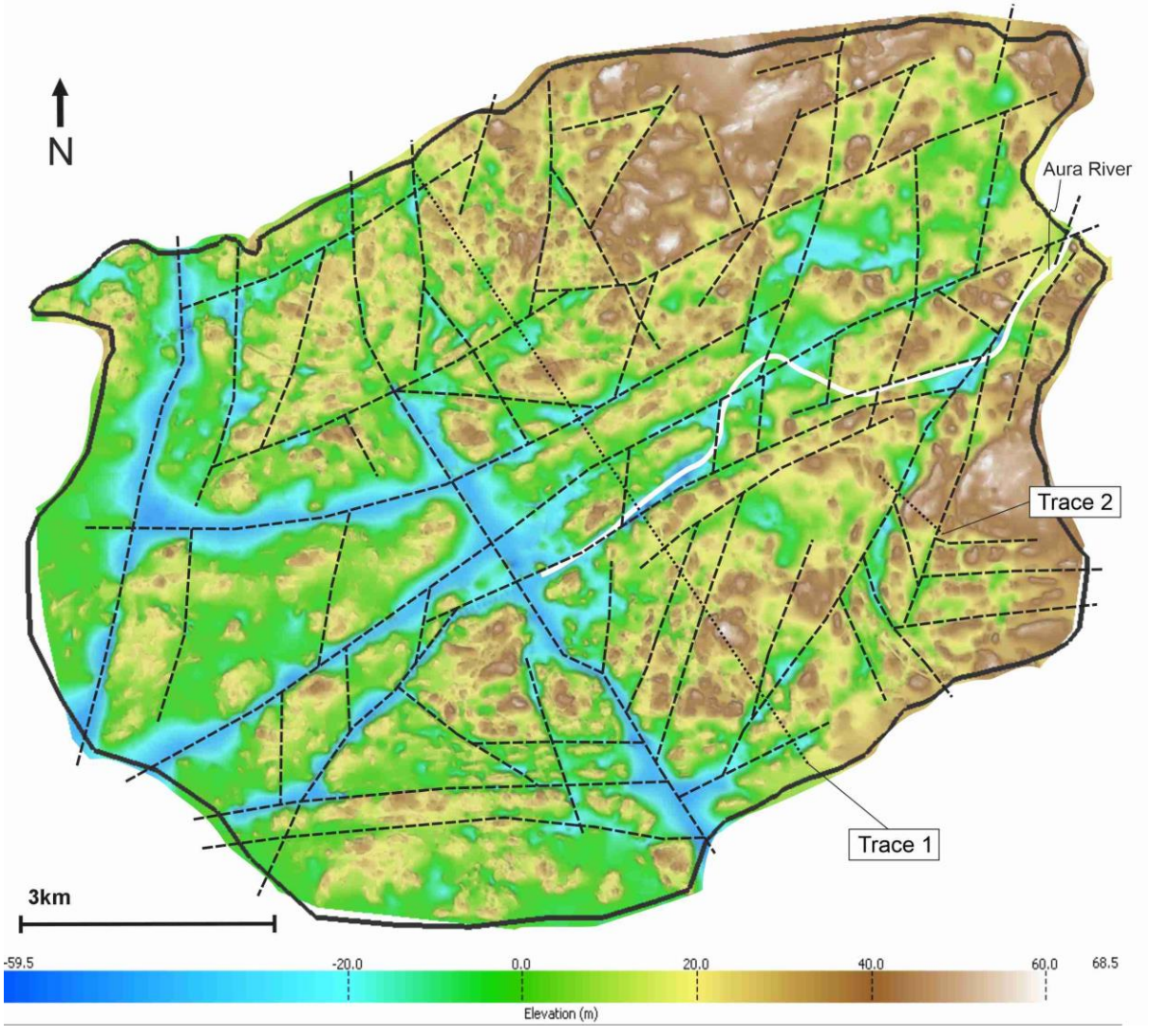

Figure 8. The bedrock-DEM and the elongated bedrock depressions (dashed lines). Interpretation further developed from Ahlqvist et al. 2025

290

4.6 Relationship between the brittle structures

https://doi.org/10.5194/egusphere-2025-4271
Preprint. Discussion started: 12 September 2025

R1-fractures strike mainly NNE to NNW, which do not correspond with the prevailing trends of lidar lineaments and bedrock depressions despite of the minor overlap distinguished from the 2D-photogrammetry model, where the R1-fractures strike NNE. R2-fracture measurements (Fig. 6d) show clustered sets of ENE-, NW- and E-strike which correspond with the lidar lineaments and bedrock depressions (Fig. 6a, 8).

The general setting of lidar lineaments varies between north and south part of the study area divided by the continuous ENE-striking SZ1 and SZ2 (Fig. 3, 6). The north part is characterized by more varying lidar lineament and bedrock depression trends while NNE- to NE-striking trends are the most characteristic in the south part together with the E-striking trend (Fig. 6a, 8). Lidar lineaments strike parallel along the ENE-striking shear zones (SZ1-3), but same parallelism between lineaments and NE- and NW-striking faults is much weaker.

The trends of bedrock depressions correspond with the lidar lineaments, and most continuous and deepest bedrock depressions are located along the shear zones and faults (Fig. 9a). Continuous ENE-striking bedrock depressions are located along SZ1 and SZ2. The NNE to NE-striking bedrock depressions are continuous particularly along the F2 and ASZ, but elsewhere, they tend to terminate to the ENE-striking bedrock depressions. Despite of the limited extent, the bedrock depressions with NNE to NE-strike are the most commonly featured throughout the study area same as the parallel lidar lineaments. Most distinct NW-striking bedrock depression is located along the F1, which intersects with the long ENE-striking depressions in the central part of the study area. NNE- to NE- striking bedrock depressions are featuring the bedrock surface morphology on the north side even though the parallel lineaments are not as prevailing as in the south. South side of the SZ2 show also heterogeneous brittle structural pattern but the NNE- to NE lineaments are dominant feature together with the parallel bedrock depressions. Fig. 9a shows the overall relationship of the lidar lineaments and bedrock depression with major shear zones and faults. This overall relationship of brittle structures addressed in the Fig. 9b, shows the comprehensive network of shear zones and faults (black solid lines) together with fracture measurements (red lines) and distinctive bedrock depressions, which are not interpreted as deformation zones (black dashed lines) due to their weaker contrast in the bedrock elevation or discontinuous character.

https://doi.org/10.5194/egusphere-2025-4271
Preprint. Discussion started: 12 September 2025

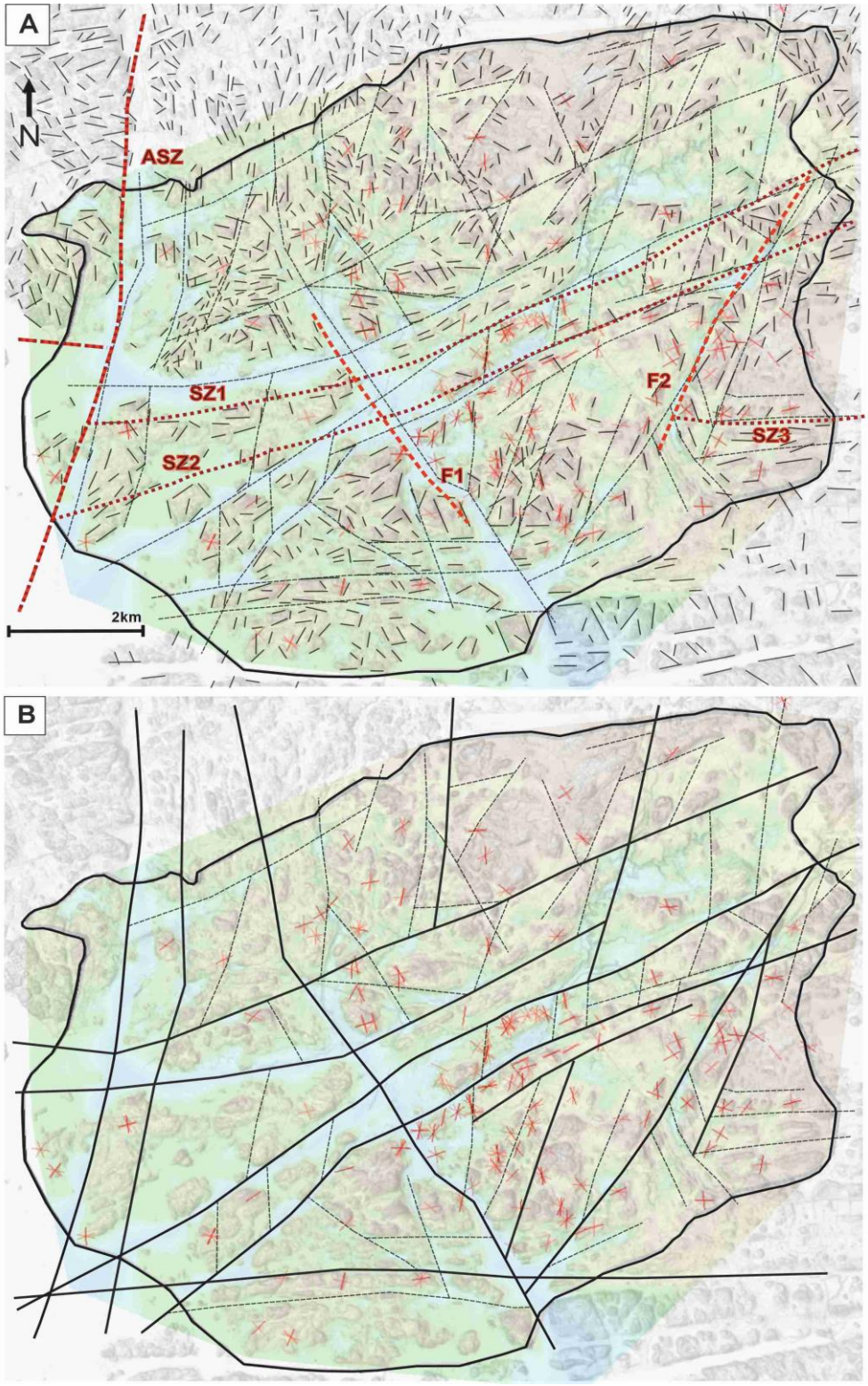

Figure 9. Compilation of brittle structures and their relationship with shear zones and faults. Ground surface LiDAR and Bedrock-DEM on the background (transparent colour map equivalent with the Fig. 8). Black dashed lines = elongated bedrock depressions, red lines= fracture measurements. A) Shear zones 1-3 (red-dotted lines) and Faults 1-2 (red-dashed lines) detected from the low-altitude aeromagnetic data and lidar lineaments = black lines, B) The network of shear zones and faults (Black solid lines).

https://doi.org/10.5194/egusphere-2025-4271
Preprint. Discussion started: 12 September 2025

4.7 Structural analysis within cross-section DEMs

4.7.1 T1-DEM

The SSE-side of T1-DEM is controlled by ENE-striking and SSE-dipping subvertical foliation, whereas, the NNW-part is characterized by isoclinal to open folding representing high- and low-strain areas, respectively. Low-strain area is characterized by gently dipping foliations within the openly folded antiform, wheareas in the high-strain areas, foliation is subvertical. Low-strain area comprises openly folded antiform-structure (OA in Fig. 10a,e,f) surrounded by high-strain areas of isoclinal folding in the NNW, and within the ENE trending shear zones in the SSE. Cross-section of the Trace 1 ascertains that the shear zone, which occurs along the Aura River depression and, coincides spatially with the deepest part of the bedrock surface, acts as a boundary for different foliation and fracture systems on the SSE- and NNW-side.

Fractures within T1-DEM area appear mostly subvertical, but sparse gently-dipping fractures are present in the low-strain areas and near Aura River shear zone. Subvertical R1-fractures generate two distinct NNE- and NNW-striking sets (Fig. 10c), while R2-fracturing strike more towards NE and NW (Fig.10d). NNE- and NNW-striking fractures are present throughout the T1-DEM, but they show significant volume within the damage zone of SZ2 (black lineaments; Fig.10b). NNE- and NNW-striking fractures are prevailing on the south side of the SZ2, but they get more irregular towards north from the Aura River shear zone (Fig. 10a). NW- and NE-striking R2-fractures occur regularly throughout the T1-DEM indicating that the Aura River shear zone does not affect these fracture trends.

Elevation of the bedrock surface shows variations within T1-DEM from -59.6 to 64.7 m.a.s.l, nearly equalling to the elevation range of the whole bedrock-DEM. The deepest part of T1-DEM is located along the Aura River shear zone but low elevation is also reached along the other ENE-striking shear zones (Fig. 10a). Furthermore, low-lying bedrock elevation is observed in the SSE-part of T1-DEM, where several continuous NNE-, NE- and E-striking bedrock depressions (Fig. 10a). The NNE-striking depression may act as a diminished continuation of the NE-striking fault within the T2-DEM.

4.7.2 T2-DEM

NNW- to N-striking fractures are the prevailing R1-fracture orientation and those are localized near Jaaninoja Fault (Fig. 11b,c). NE-striking fractures are the most frequent fracture set within T2-DEM displayed in both R1 and R2 classes (Fig. 11c,d). NE-striking fractures occur regularly throughout T2-DEM but without any significant spatial concentration. E-striking R2-fractures occur on the southern part of the T2-DEM mainly as a subsidiary fracturing.

https://doi.org/10.5194/egusphere-2025-4271
Preprint. Discussion started: 12 September 2025

Bedrock elevation in T2-DEM shows major bedrock depressions striking NNE along the Jaaninoja Fault, where elevation reaches the depth of -35 m.a.s.l. (Fig. 11a,b). Roughness of the bedrock surface is also emphasized by the E-striking small-scale bedrock depressions in the southern part of T2-DEM. Bedrock elevation shows much weaker contrast along the E-branch of the fault, where the interpolated bedrock surface is located falsely above the ground surface due to lack of bedrock surface data (Fig. 11e). Even with the detailed interpolation method of T2-DEM, "estimated" bedrock surface is often located significantly deeper along the brittle bedrock structures if the data coverage is not exceptionally comprehensive.

https://doi.org/10.5194/egusphere-2025-4271
Preprint. Discussion started: 12 September 2025

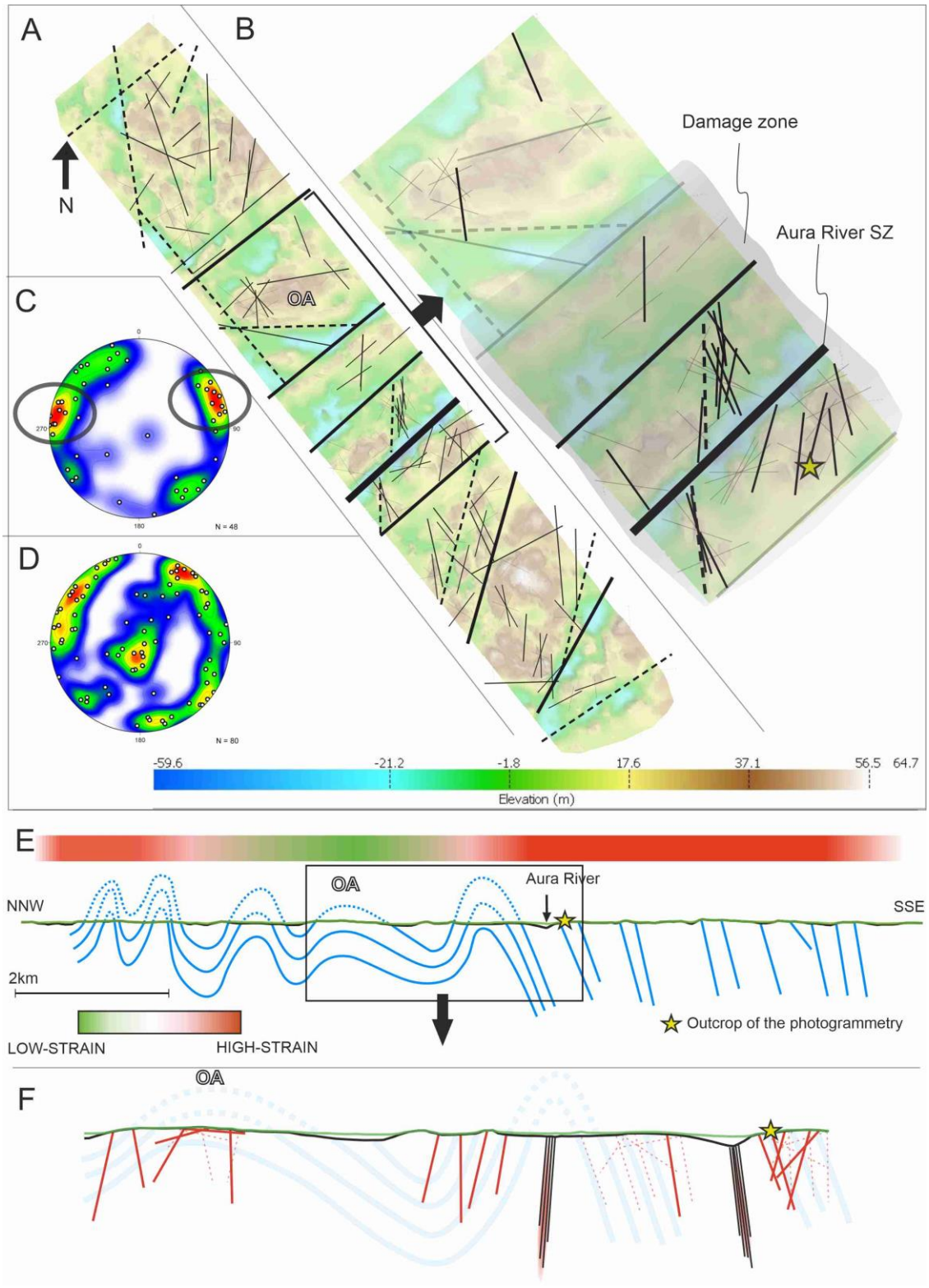

Figure 10. A) T1-DEM with brittle structures and shear zones. Black bolded lines = shear zones and faults, Black dashed lines = bedrock depressions, black thin lines = integration of lidar lineaments and fractures. B) Orientation of the brittle structures near Aura River shear zone (NNE to NNW-striking brittle structures bolded) C) R1-fractures within T1-DEM (NNE- to NNW-striking fractures circled in the stereoplot). D) R2-fractures within T1-DEM. E) Cross-section along T1-DEM (Trace 1) with foliation orientations and high/low-strain areas. F) Cross-section with fracture orientation and shear zones. R1-fractures = red lines, R2-fractures = dotted red lines, shear zones (SZ1 and SZ2) = black line swarm, bedrock surface = black line, ground surface = green line.

https://doi.org/10.5194/egusphere-2025-4271
Preprint. Discussion started: 12 September 2025

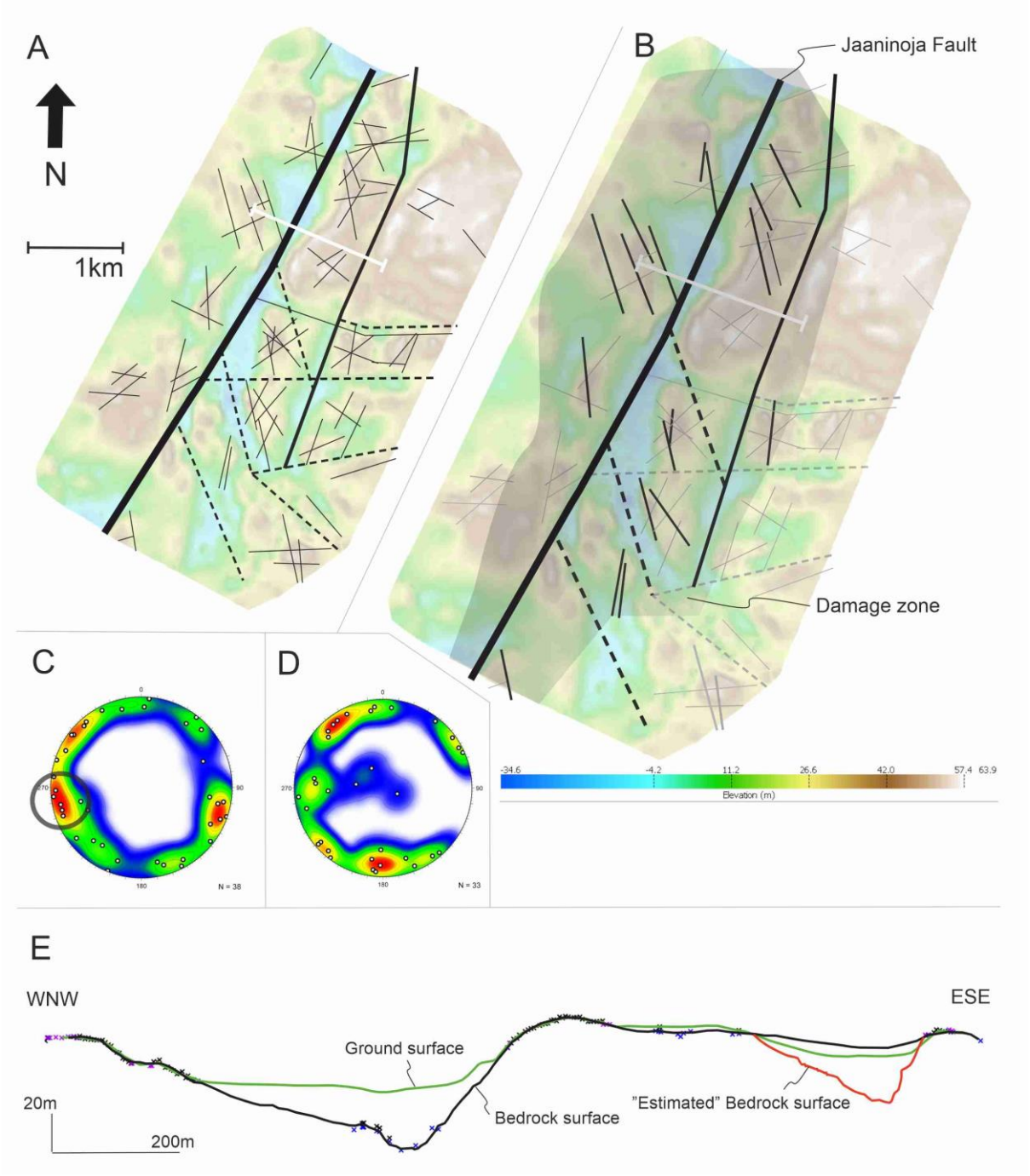

Figure 11. A) Brittle structures within the T2-DEM. Black bolded lines = faults, Black dashed lines = bedrock depressions, black thin lines = integration of lidar lineaments and fractures. B) NNW-striking brittle structures highlighted near Jaaninoja fault. C) R1-fractures (circled area correspond the brittle structures highlighted in the Fig. B). D) R2-fractures. E) Cross-section across F1 emphasizes the difference of ground surface and bedrock surface (Z-value exaggerated x3,5). Note the inaccurate interpolation of the bedrock surface in the ESE-part of the cross-section, which lack bedrock surface data points.

https://doi.org/10.5194/egusphere-2025-4271
Preprint. Discussion started: 12 September 2025

360

4.8 Summary of the relationship between bedrock structures and the bedrock surface

Ductile structures generate a systematic ENE-striking structural framework into the bedrock for the later brittle deformation, but the brittle structures show much complex setting, and their prevailing orientation do not follow the ductile framework 365 nor the lithological boundaries extensively within the study area. Our results show that the lidar lineaments, faults and shear zones correlate with the topographic signatures detected from the bedrock-DEM. However, there are no ductile or larger-scale brittle structural precursor for the NNW- and NNE-striking R1-fractures which indicates, that these fractures are formed as response of the movement in the deformation zones. Cross-section DEMs illustrate that Aura River shear zone and Jaaninoja fault control the spatial occurrence of these fractures by bordering and emphasising the NNW to NNE-striking 370 fractures within the damage zones. The R2-fractures show similar ENE-strike than the foliation and shear zones, which suggest that the R2-fractures were largely localized into the existing ductile structures particularly near the ENE-striking shear zones.

Intensive NNE- and secondary NW-striking fractures in the 2D-photogrammetry model correlate well with observed R1- and R2-fracture orientation along Aura River shear zone (Fig. 10) together with the overall fracturing trends within the study 375 area (Fig. 7). The fracture sets in the photogrammetry model also correspond with R1/R2 orientations within T1-DEM. Therefore, outcrop of the photogrammetry model is located within the damage zone of Aura River shear zone due to high intensity of the NNE-striking fractures indicating, that the damage zone width reaches at least 400m. Since the NNE- to NNW-striking fractures are prevailing within the shear zones and faults, they also control the detailed morphology of the bedrock depression slopes. T2-DEM and the associated structural analysis are conducted along Jaaninoja fault, which show 380 that the bedrock depressions slopes are irregular, controlled by the prevailing fracture trend. Along the shear zones and faults, the bedrock surface is featured by the elongate bedrock depressions but with different surface morphology. Bedrock depressions associated with the ENE-striking shear zones and NW-striking faults are wider in character compared to the bedrock depression along the NE-striking faults in the T2-DEM. This, and the structural analysis of the cross-section DEMs indicates that the damage zone width along the shear zones is generally wider than along the faults (Fig, 12).

https://doi.org/10.5194/egusphere-2025-4271
Preprint. Discussion started: 12 September 2025

Figure 12. The network of shear zones and faults, and their assumed damage zones (=areas without white mask).

5. Discussion

https://doi.org/10.5194/egusphere-2025-4271
Preprint. Discussion started: 12 September 2025

5.1. Networking and kinematics of the main shear zones and faults

The network of shear zones and faults shows that the large-scale brittle structures generate much more complex setting than the ductile framework within the study area (Fig. 12). Shear zones, following the ductile framework of the bedrock, are concentrated in the central and southern parts of the study area striking ENE and E, respectively. The setting of large-scale brittle structures is characterized by NNE- to NE-striking faults distinguished widely throughout the study area together with NW-striking fault that separates the mainland from the archipelago in the central parts.

Cross-section DEMs show increasing number of NNE- and NNW-striking lidar lineaments and fractures (black solid lines in Fig. 10b, 11b) within the damage zone of Aura River shear zone (T1-DEM) and Jaaninoja fault (T2-DEM), which indicate a sinistral kinematic system, where the NNE- and NNW-striking fractures (orange solid lines in Fig. 13) represent tension fractures formed aligned with the main stress orientation.

Aura River shear zone is associated with parallel fracture set within the damage zone but also host the system of Riedel and tension fractures (Fig. 13). Fracture system along Jaaninoja fault features the system of Riedel and tension fractures with only sporadic fault-parallel fractures. Therefore, the NNW-striking and NNE-striking tension fractures within Aura River shear zone and Jaaninoja faults correspond with the prevailing stress regimes occurred in southwestern Finland (Fig. 13), while the ENE-striking fractures are reactivated from ductile framework in the damage zone of the Aura River shear zones. Although the shear zones and faults are covered by water and sediment deposits that prevents the direct observations, fracture network within the exposed damage zones of Aura River shear zone and Jaaninoja fault act as evidence for the sinistral kinematics.

In the early stages after the onset of brittle deformation (Stage 1 & 2; c.1.75 – 1.65 Ga; Mattila & Viola, 2014), NNW- and NNE-oriented compressional stress regime prevailed in southwestern Finland. NNE-oriented compressional stress regime corresponds well with brittle structural setting, and the resulting kinematic interpretation along the Aura River shear zone, while the NNW-oriented compression supports the kinematic interpretation along Jaaninoja fault (Fig. 13). As such, the timing of faulting and the development of the damage zone along the Aura River shear zone may be constrained to the early stages of the brittle crustal evolution at around 1.75 Ga (Mattila & Viola, 2014) that followed the main 1.9-1.8 Ga Svecofennian orogenic evolution. Consequently, the reported later brittle events and reactivations at 1.64 Ga (Torvela et al., 2008; Torvela & Kurhila, 2022; Nordbäck, et al., 2024) had no major effect on the deformation zones in the study area, or their potential effect is delimited to the unexposed core-domains.

https://doi.org/10.5194/egusphere-2025-4271
Preprint. Discussion started: 12 September 2025

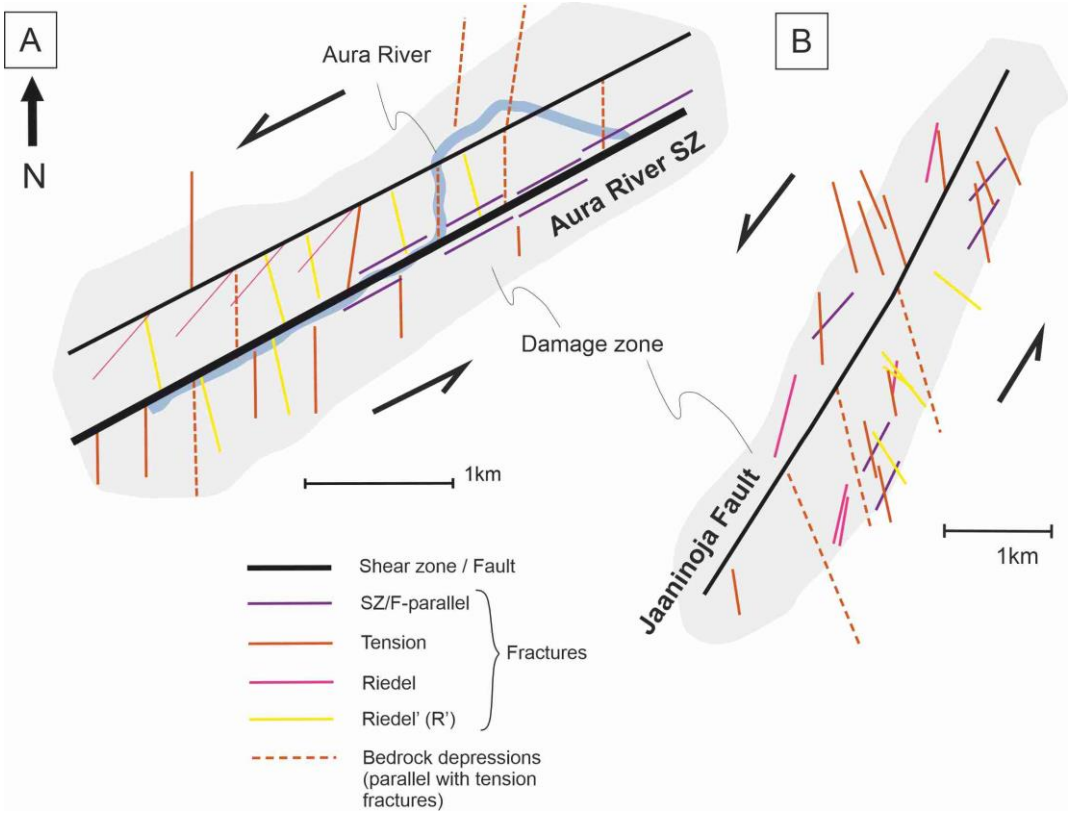

Figure 13. Simplified sketch of brittle structures and kinematics along (A) Aura River shear zone and (B) the Jaaninoja Fault.

420

5.2. The influence of the brittle structures upon the surface morphology of the bedrock depressions

Our results show that the large-scale brittle structures (lineaments, faults and shear zones) interpreted from LiDAR-data and bedrock-DEM correlate with the elongated topographic depressions along the eroded bedrock surface displayed as elongate bedrock depressions. However, the slopes of the bedrock depressions show morphological irregularities in detailed scale due to prevailing NNE- to NNW-striking tension fractures within the shear zones and faults.

The Bedrock-DEM reveals that the bedrock depressions along the ENE-striking shear zones are wider than the sharp depressions along the NNE- to NE- and NW-striking faults. This suggest that the brittle over the ductile shear zones (i.e. along pre-existing ductile fabric) was more distributed than deformation along the faults with no precursors, and, consequently created wider damage zones with fragmented bedrock. The NNE to NE-striking bedrock depressions tend to

https://doi.org/10.5194/egusphere-2025-4271
Preprint. Discussion started: 12 September 2025

terminate particularly against the continuous ENE-striking depressions. The deepest parts of the bedrock elevation are at the intersections of two or more bedrock depressions, underlaid by shear zones or faults.

While the strikes of the elongate bedrock depressions correspond to the orientation of the brittle lineaments, the oblique NNW- and NNE-striking fractures control the detailed morphology in the slopes of the bedrock depressions distinguished near the shear zones and faults within T1-DEM and T2-DEM. The bedrock elevation, particularly along the T2-DEM fault, is not ascending gradually away from the fault core but creating zig-zag-patterns at the slopes of the depressions controlled by the intense NNW-striking fractures (Fig. 11b). This zig-zag-pattern is often observed from the outcrops, where the general trend of the outcrop walls is controlled by fracture sets that are striking obliquely and/or dipping to the opposite direction than the outcrop wall itself (Fig. 14a-d). The interpolated bedrock surface in the cross-sections show that the SSE-side of the depression wall along the Aura River shear zone, and the ESE-side depression wall along the Jaaninoja fault are steeper than the respective opposite slopes.

Considering the effect of glacial erosion upon the generation of the observed bedrock depressions, glacial ripping and quarrying are the main mechanisms of glacial erosion, which utilize the fragmentation of the bedrock due to closely spaced fractures within the damage zones of the shear zones and faults, and thus generates abrupt breaks onto the bedrock surface morphology (Dühnforth et al., 2010; Lane et al., 2015; Bukhari et al., 2021; Skyttä et al., 2023). Within the Turku region the width and depth of the bedrock depressions are greater along NW-striking fault than NNE- to NE-striking faults, which is likely caused by the favourable orientation of the NW-striking bedrock depressions to glacial flow direction (NW-SE). ENE-striking bedrock depression along Aura River shear zones shows deep and wide morphological character even if the depression is striking perpendicular to the glacial flow direction, which could be resulted by lee-side plucking type of processes (Krabbendam & Bradwell, 2011).

Prevailing bedrock structures and the glacial erosion processes complicate the bedrock surface morphology. Therefore, interpolation method needs to be as detailed as possible, which is achieved by throughout testing and selecting the method according to its suitability to the study area. Our interpolation method gives more precise outcome within areas of high-elevated bedrock surface, but similar accuracy cannot be achieved along the elongated bedrock depression due to lack of data points. Therefore, detailed multi-scale analysis of the bedrock structures provide often indirect, yet vital knowledge regarding the bedrock surface morphology within the bedrock depressions for generating structurally realistic bedrock-DEM.

https://doi.org/10.5194/egusphere-2025-4271
Preprint. Discussion started: 12 September 2025

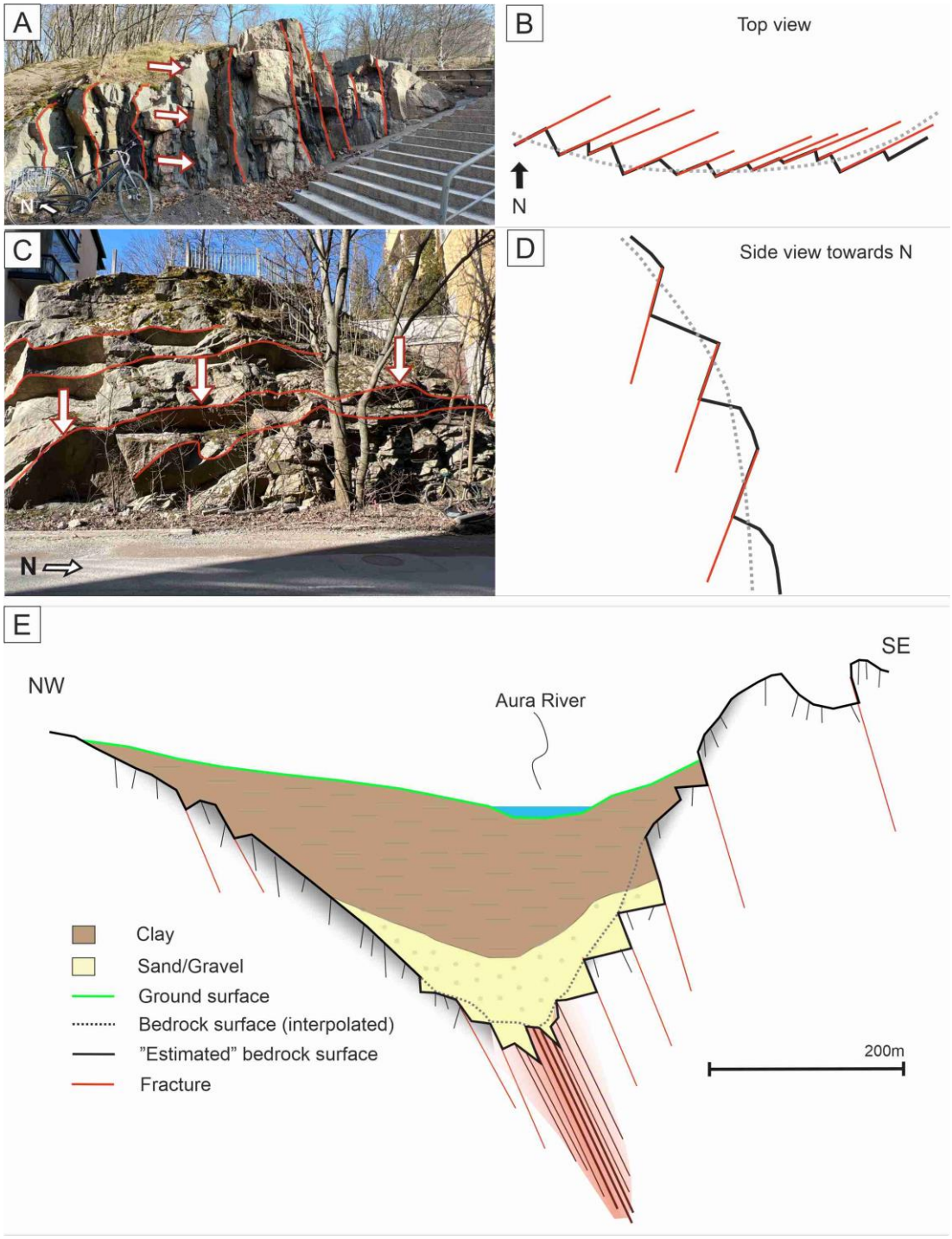

Figure 14. How fractures control the bedrock surface morphology. A) R1-fracture orientation controls the morphology of the outcrop wall in the horizontal perspective. B) A sketch of the outcrop presented in the Fig. A drawn from the top view to illustrate how the R1-fractures control the outcrop wall in the horizontal perspective. C) R1-fracture orientation controls the morphology of the outcrop wall in the vertical perspective. D) A sketch of the outcrop presented in the Fig. C drawn towards North to illustrate how the R1-fractures control the outcrop wall in the vertical perspective. E) A sketch of Aura River (SZ2; T2-DEM) depression shows how the "true" bedrock surface morphology is controlled by subvertical fractures. Z-value is exaggerated.

https://doi.org/10.5194/egusphere-2025-4271
Preprint. Discussion started: 12 September 2025

6. Conclusions

Shear zones have strong ENE-striking ductile precursors, which controls their localization and orientation whereas the faults are cross-cutting in character with respect to the ductile framework. Roughness of the bedrock surface is characterized by numerous bedrock depressions that are spatially coinciding with shear zones and faults. Lowest elevations are detected within the bedrock depressions along the core-domains of shear zone and fault, and particularly along their intersections, that define wider areas of low-elevation bedrock surfaces.

Elongated bedrock depressions show similar trends with the shear zones and faults (ENE- and NNE- to NE-striking), but prevailing outcrop-scale fractures have deviating NNE and NNW strike particularly within the damage zones of shear zones and faults, and can hence be attributed to secondary fracturing caused by the slip along the faults. NNE- and NNW-striking fractures are featured particularly near the shear zones and faults, which indicates, that they belong to the area of damage zone. Outside of the damage zones, the number of NNE- and NNW-striking fractures decrease and the general fracture setting correspond the dominant trends of the shear zones and faults.

Cross-section-DEMs show that the NNE- and NNW-striking fractures control the trend of the bedrock depressions slopes within the damage zones by generating more zig-zag patterns than linear slopes. Since the bedrock surface is controlled by subvertical R1-fractures, and also the other bedrock structures show subvertical-nature, the “true” bedrock surface within the bedrock depressions is rougher and containing abrupt breaks that the interpolations cannot detect.

Authorship contribution:

ER: design of the study, methodology, fieldwork, data acquisition, data interpretation, writing the original draft, drafting of figures

PS: design of the study, methodology, fieldwork, data acquisition, data interpretation, writing

KA: design of the study, methodology, data interpretation, writing

NN: fieldwork, data acquisition, data interpretation

PB: fieldwork, data acquisition, data interpretation

KN: fieldwork, data acquisition, writing

https://doi.org/10.5194/egusphere-2025-4271
Preprint. Discussion started: 12 September 2025

Acknowledgements

Eemi Ruuska has been funded by Maa- ja Vesitekniikan Tuki Ry (19-9906-10). We thank the people of Structural Geology Group in Turku who participate to the field mapping.

References

Aeromagnetic anomaly map of Finland, 1972–2007. Version 1.0. Geological Survey of Finland, HAKKU service.

Ahlqvist, K. M., Skyttä, P., Anttila N., Ojala, A.E.K.,4, Ruuska, E.. Integration of geotechnical drillings and terrain topography into geological 3D models in the city of Turku, SW Finland. *(in prep.)*

Bedrock of Finland 1:200 000, 2022. Version 2.3. Geological Survey of Finland, HAKKU service.

Bertrand, L., Géraud, Y., Le Garzic, E., Place, J., Diraison, M., Walter, B., & Haffen, S. (2015). A multiscale analysis of a fracture pattern in granite: A case study ofthe Tamariu granite, Catalunya, Spain. *Journal of Structural Geology*, *78*, 52–66. https://doi.org/10.1016/j.jsg.2015.05.013

Bogdanova, S., Gorbatschev, R., Skridlaite, G., Soesoo, A., Taran, L., & Kurlovich, D. (2015). Trans-baltic palaeoproterozoic correlations towards the reconstruction of supercontinent Columbia/Nuna. *Precambrian Research*, *259*, 5–33. https://doi.org/10.1016/j.precamres.2014.11.023

Bukhari, S., Eyles, N., Sookhan, S., Mulligan, R., Paulen, R., Krabbendam, M., & Putkinen, N. (2021). Regional subglacial quarrying and abrasion below hard-bedded palaeo-ice streams crossing the Shield–Palaeozoic boundary of central Canada: the importance of substrate control. *Boreas*, *50*(3), 781–805. https://doi.org/10.1111/bor.12522

Chabani, A., Trullenque, G., Ledésert, B. A., & Klee, J. (2021). Multiscale characterization of fracture patterns: A case study of the noble hills range (Death valley, CA, Usa), application to geothermal reservoirs. *Geosciences (Switzerland)*, *11*(7). https://doi.org/10.3390/geosciences11070280

Healy, D., Rizzo, R. E., Cornwell, D. G., Farrell, N. J. C., Watkins, H., Timms, N. E., Gomez-Rivas, E., & Smith, M. (2017). FracPaQ: A MATLAB™ toolbox for the quantification of fracture patterns. *Journal of Structural Geology*, *95*, 1–16. https://doi.org/10.1016/j.jsg.2016.12.003

Holder, J. G. (2015). The initiation of brittle faults in crystalline rock. In *Journal of Structural Geology* (Vol. 77, pp. 159–174). Elsevier Ltd. https://doi.org/10.1016/j.jsg.2015.05.001

DesRoches, A., Danielescu, S., & Butler, K. (2014). Contrôles structuraux sur les écoulements souterrains d'un aquifère de roche fracturée au droit d'une région agricole au nord-ouest de New Brunswick au Canada. *Hydrogeology Journal*, *22*(5), 1067–1086. https://doi.org/10.1007/s10040-014-1134-0

Michiarante, A. M., McCaffrey, K. J. W., Holdsworth, R. E., Bjørnarå, T. I., & Dempsey, E. D. (2020). Fracture attribute scaling and connectivity in the Devonian Orcadian Basin with implications for geologically equivalent sub-surface fractured reservoirs. *Solid Earth*, *11*(6), 2221–2244. https://doi.org/10.5194/se-11-2221-2020

Dühnforth, M., Anderson, R. S., Ward, D., & Stock, G. M. (2010). Bedrock fracture control of glacial erosion processes and rates. *Geology*, *38*(5), 423–426. https://doi.org/10.1130/G30576.1

Rutanders, C., Lindroos, A., & Selonen, O. (1993). The late Svecofennian granite-migmatite zone of southern Finland a belt of transpressive deformation and granite emplacement. In *Precambrian Research* (Vol. 64).

https://doi.org/10.5194/egusphere-2025-4271
Preprint. Discussion started: 12 September 2025

Eyles, N. (2012). Rock drumlins and megaflutes of the Niagara Escarpment, Ontario, Canada: a hard bed landform assemblage cut by the Saginaw-Huron Ice Stream. *Quaternary Science Reviews*, *55*, 34–49. https://doi.org/10.1016/j.quascirev.2012.09.001

Glasser, N. F., Crawford, K. R., Hambrey, M. J., Bennett, M. R., & Huddart, D. (1998). *Lithological and Structural Controls on the Surface Wear Characteristics of Glaciated Metamorphic Bedrock Surfaces: Ossian Sarsfjellet, Svalbard 1*. http://www.journals.uchicago.edu/t-and-c

Glasser, N. F., Roman, M., Holt, T. O., Žebre, M., Patton, H., & Hubbard, A. L. (2020). Modification of bedrock surfaces by glacial abrasion and quarrying: Evidence from North Wales. *Geomorphology*, *365*. https://doi.org/10.1016/j.geomorph.2020.107283

Gleeson, T., & Novakowski, K. (2009). Identifying watershed-scale barriers to groundwater flow: Lineaments in the Canadian shield. *Bulletin of the Geological Society of America*, *121*(3–4), 333–347. https://doi.org/10.1130/B26241.1

Hall, A. M., & Gillespie, M. R. (2017). Fracture controls on valley persistence: the Cairngorm Granite pluton, Scotland. *International Journal of Earth Sciences*, *106*(6), 2203–2219. https://doi.org/10.1007/s00531-016-1423-z

Hardebol, N. J., Maier, C., Nick, H., Geiger, S., Bertotti, G., & Boro, H. (2015). Multiscale fracture network characterization and impact on flow: A case study on the Latemar carbonate platform. *Journal of Geophysical Research: Solid Earth*, *120*(12), 8197–8222. https://doi.org/10.1002/2015JB011879

Hermansson, T., Stephens, M. B., Corfu, F., Page, L. M., & Andersson, J. (2008). Migratory tectonic switching, western Svecofennian orogen, central Sweden: Constraints from U/Pb zircon and titanite geochronology. *Precambrian Research*, *161*(3–4), 250–278. https://doi.org/10.1016/j.precamres.2007.08.008

Hietanen, A. (1947). Archean geology of the Turku district in southwestern Finland. Geological Society of America Bulletin, 58(11), 1019-1084.

Huhma, H. (1986). Sm-Nd, U-Pb and Pb-Pb isotopic evidence for the origin of the Early Proterozoic Svecokarelian crust in Finland. Geol. Surv. Finland Bull., 337.

Härme, M. (1960). Suomen geologinen yleiskartta. The general geological map of Finland. Lehti-Sheet B 1. Kivilajikartan selitys. English summary.

Kirkpatrick, J. D., Bezerra, F. H. R., Shipton, Z. K., Do Nascimento, A. F., Pytharouli, S. I., Lunn, R. J., & Soden, A. M. (2013). Scale-dependent influence of pre-existing basement shear zones on rift faulting: A case study from NE Brazil. *Journal of the Geological Society*, *170*(2), 237–247. https://doi.org/10.1144/jgs2012-043

Korsman, K., Koistinen, T., Kohonen, J., Wennerström, M., Ekdahl, E., Honkamo, M., ... & Pekkala, Y. (1997). Suomen kallioperäkartta= Berggrundskarta över Finland= Bedrock map of Finland. Geological Survey of Finland, Espoo, Finland.

Krabbendam, M., Hall, A. M., Palamakumbura, R. M., & Finlayson, A. (2022). Glaciotectonic disintegration of roches moutonnées during glacial ripping in east Sweden. *Geografiska Annaler, Series A: Physical Geography*, *104*(1), 35–56. https://doi.org/10.1080/04353676.2021.2022356

Kurhila, M., Vaasjoki, M., Mänttäri, I., Rämö, T., & Nironen, M. (2005). U-Pb ages and Nd isotope characteristics of the lateorogenic, migmatizing microcline granites in southwestern Finland. *Bulletin of the Geological Society of Finland*, *77*(2), 105–128. https://doi.org/10.17741/bgsf/77.2.002

Lahtinen, Y. (2005). *Chapter 8 Svecofennian supracrustal rocks* (pp. 343–405). https://doi.org/10.1016/S0166-2635(05)80009-X

Lahtinen, R., Korja, A., Nironen, M., & Heikkinen, P. (2009). Palaeoproterozoic accretionary processes in Fennoscandia. *Geological Society Special Publication*, *318*, 237–256. https://doi.org/10.1144/SP318.8

Lane, T. P., Roberts, D. H., Rea, B. R., Cofaigh, C., & Vieli, A. (2015). Controls on bedrock bedform development beneath the Uummannaq Ice Stream onset zone, West Greenland. *Geomorphology*, *231*, 301–313. https://doi.org/10.1016/j.geomorph.2014.12.019

https://doi.org/10.5194/egusphere-2025-4271
Preprint. Discussion started: 12 September 2025

560 ser scanning data of ground surface (LiDAR), 2008-2019. National Land Survey of Finland

Mancktelow, N. S., & Pennacchioni, G. (2005). The control of precursor brittle fracture and fluid-rock interaction on the development of single and paired ductile shear zones. *Journal of Structural Geology*, *27*(4), 645–661. https://doi.org/10.1016/j.jsg.2004.12.001

Mattila, J., & Viola, G. (2014). New constraints on 1.7Gyr of brittle tectonic evolution in southwestern Finland derived from a structural study at the site of a potential nuclear waste repository (Olkiluoto Island). *Journal of Structural Geology*, *67*(PA), 50–74. 565 https://doi.org/10.1016/j.jsg.2014.07.003

Niemelä, J., Stén, C-G., Taka, M. & Winterhalter, B. 1987. Turun-Salon seudun maaperä. Maaperäkarttojen selitykset, lehdet 1043 ja 2021. Suomen geologinen kartta, 1:100 000. Geologian tutkimuskeskus, Espoo. 83 s.

Nironen, M. (2017). Guide to the geological map of Finland–Bedrock 1: 1 000 000. Geological Survey of Finland, Special Paper, 60, 41-76.

Nordbäck, N., Ovaskainen, N., Markovaara-Koivisto, M., Skyttä, P., Ojala, A., Engström, J., & Nixon, C. (2023). Multiscale mapping and 570 scaling analysis of the censored brittle structural framework within the crystalline bedrock of southern Finland. *Bulletin of the Geological Society of Finland*, *95*(1), 5–32. https://doi.org/10.17741/bgsf/95.1.001

Nordbäck, N., Skyttä, P., Engström, J., Ovaskainen, N., Mattila, J., & Aaltonen, I. (2024). Mesoproterozoic Strike-Slip Faulting within the Åland Rapakivi Batholith, Southwestern Finland. *Tektonika*, *2*(1). https://doi.org/10.55575/tektonika2024.2.1.51

Ovaskainen, N., Nordbäck, N., Skyttä, P., & Engström, J. (2022). A new subsampling methodology to optimize the characterization of two-575 dimensional bedrock fracture networks. *Journal of Structural Geology*, *155*. https://doi.org/10.1016/j.jsg.2022.104528

Regenauer-Lieb, K., & Yuen, D. A. (2008). Multiscale brittle-ductile coupling and genesis of slow earthquakes. *Pure and Applied Geophysics*, *165*(3–4), 523–543. https://doi.org/10.1007/s00024-008-0326-8

Ruuska, E., Skyttä, P., Putkinen, N., & Valjus, T. (2023). Contribution of bedrock structures to the bedrock surface topography and groundwater flow systems within deep glaciofluvial aquifers in Kurikka, Western Finland. *Earth Surface Processes and Landforms*, *48*(10), 2039–2056. 580 https://doi.org/10.1002/esp.5602

Samsu, A., Cruden, A. R., Micklethwaite, S., Grose, L., & Vollgger, S. A. (2020). Scale matters: The influence of structural inheritance on fracture patterns. *Journal of Structural Geology*, *130*. https://doi.org/10.1016/j.jsg.2019.103896

Sanderson, D. J., & Nixon, C. W. (2015). The use of topology in fracture network characterization. *Journal of Structural Geology*, *72*, 55–66. https://doi.org/10.1016/j.jsg.2015.01.005

585 tt, D. N., & Wohl, E. E. (2019). Bedrock fracture influences on geomorphic process and form across process domains and scales. In *Earth Surface Processes and Landforms* (Vol. 44, Issue 1, pp. 27–45). John Wiley and Sons Ltd. https://doi.org/10.1002/esp.4473

Simelius, C. 2013. Airiston hiertovyöhyke – Duktiilista deformaatiosta hauraiden rakenteiden ympäristöksi. Master thesis, University of Turku, Department of Geography and Geology, 93 s.

Skyttä, P., Kinnunen, J., Palmu, J. P., & Korkka-Niemi, K. (2015). Bedrock structures controlling the spatial occurrence and geometry of 1.8Ga 590 younger glacifluvial deposits - Example from First Salpausselkä, southern Finland. *Global and Planetary Change*, *135*, 66–82. https://doi.org/10.1016/j.gloplacha.2015.10.007

Skyttä, P., Nordbäck, N., Ojala, A., Putkinen, N., Aaltonen, I., Engström, J., Mattila, J., & Ovaskainen, N. (2023). The interplay of bedrock fractures and glacial erosion in defining the present-day land surface topography in mesoscopically isotropic crystalline rocks. *Earth Surface Processes and Landforms*, *48*(10), 1956–1968. https://doi.org/10.1002/esp.5596

595 kyttä, P., & Torvela, T. (2018). Brittle reactivation of ductile precursor structures: The role of incomplete structural transposition at a nuclear waste disposal site, Olkiluoto, Finland. *Journal of Structural Geology*, *116*, 253–259. https://doi.org/10.1016/j.jsg.2018.06.009

https://doi.org/10.5194/egusphere-2025-4271
Preprint. Discussion started: 12 September 2025

Suominen, V. (1991). The chronostratigraphy of southwestern Finland with special reference to Postjotnian and Subjotnian diabases. Bulletin-Geological Survey of Finland, (356).

Torvela, T., & Ehlers, C. (2010). From ductile to brittle deformation: Structural development and strain distribution along a crustal-scale shear zone in SW Finland. *International Journal of Earth Sciences*, *99*(5), 1133–1152. https://doi.org/10.1007/s00531-009-0451-3

Torvela, T., & Kurhila, M. (2022). Timing of syn-orogenic, high-grade transtensional shear zone formation in the West Uusimaa Complex, Finland. *Bulletin of the Geological Society of Finland*, *94*(1), 5–22. https://doi.org/10.17741/bgsf/94.1.001

Torvela, T., Mänttäri, I., & Hermansson, T. (2008). Timing of deformation phases within the South Finland shear zone, SW Finland. *Precambrian Research*, *160*(3–4), 277–298. https://doi.org/10.1016/j.precamres.2007.08.002

Väisänen, M., & Hölttä, P. (1999). Structural and metamorphic evolution of the Turku migmatite complex, southwestern Finland. Bulletin of the Geological Society of Finland, 71(1), 177-218.

Väisänen, M., & Skyttä, P. (2007). *Late Svecofennian shear zones in southwestern Finland*, Gff, Vol. 129, 55-64.